2015 SNMMI Highlights Lecture: Oncology, Part II

Umar Mahmood, MD, PhD, Massachusetts General Hospital, Boston, MA

From the Newsline Editor: *The Highlights Lecture, presented at the closing session of each SNMMI Annual Meeting, was originated and delivered for more than 30 years by Henry N. Wagner, Jr., MD. Beginning in 2010, the duties of summarizing selected significant presentations at the meeting were divided annually among 4 distinguished nuclear and molecular medicine subject matter experts. The 2015 Highlights Lectures were delivered on June 10 at the SNMMI Annual Meeting in Baltimore, MD. Umar Mahmood, MD, PhD, Professor of Radiology at Massachusetts General Hospital (Boston, MA), spoke on oncology highlights from the meeting's sessions. Because of its length, the oncology presentation is divided between 2 Newsline issues. Part I was published in the November issue. Note that in the following summary, numerals in brackets represent abstract numbers as published in* The Journal of Nuclear Medicine *[2015;56:suppl 3].*

At this year's SNMMI Annual Meeting we have seen interesting work with growing numbers of tracers—both novel agents and innovative applications for tracers that are already familiar. One example is in hepatocellular cancer (HCC), where grades B and C carcinoma (intermediate grades) may be treated with ^{90}Y-selective internal radiation therapy (^{90}Y-SIRT). The predictive role of pretreatment ^{18}F-FDG PET/CT in ^{90}Y-SIRT for inoperable HCC patients with ^{18}F-FDG–avid tumors is well documented. However, it is not well studied in HCC cases that are non-avid, because these lesions may also include non-HCC cirrhotic nodules lumped together as a single "^{18}F-FDG–non-avid" category by others. Chen et al. from the Hong Kong Sanatorium and Hospital reported that "^{18}F-FDG and ^{11}C-acetate PET/CT predicts treatment response and survival of cohort of Barcelona Clinic Liver Cancer B-C patients treated with ^{90}Y-SIRT" [573]. These researchers looked at the value of ^{11}C-acetate and ^{18}F-FDG PET/CT for prediction of treatment efficacy and posttreatment survival in 18 patients referred for imaging within 2 weeks before ^{90}Y-SIRT. PET/CT with both tracers was performed at 2 months after treatment. On pretreatment imaging, 8 patients showed ^{11}C-acetate avidity and 10 showed ^{18}F-FDG avidity. All 8 (100%) of the patients with ^{11}C-acetate avidity proved to be good responders to treatment, whereas only 5 (50%) with ^{18}F-FDG avidity had good responses. Metabolic poor/good response as assessed on follow-up PET/CT was a significant predictor for 2-year overall survival in these patients. Figure 1 shows examples from this study. On the left are follow-up (top) and baseline (bottom) ^{18}F-FDG and ^{11}C-acetate images from a patient with ^{11}C-acetate–avid HCC who went on to a good treatment response, with survival >24 months. On the right are corresponding images from a patient with ^{18}F-FDG–avid HCC but without ^{11}C-acetate avidity who died 9 months after treatment. Whether a tumor is more fatty acid dependent or glucose dependent may help to characterize its genetic makeup or its phenotype and inform subsequent treatment strategies.

Umar Mahmood, MD, PhD

Brain tumors can be assessed in many ways, and a recent body of exciting work looks at the potential of amino acid imaging. One of the challenges in brain metastasis imaging is in differentiating tumor recurrence from radiation necrosis. Guffens et al. from Universitaire Ziekenhuizen Leuven–Katholieke Universiteit Leuven (Belgium) reported that "Dynamic O-(2-^{18}F-fluoroethyl)-l-tyrosine (^{18}F-FET) PET improves differentiation of local recurrent brain metastasis from radiation necrosis" [628]. Only limited data are available on the value of dynamic ^{18}F-FET PET in such differentiation. In this retrospective analysis, the researchers looked at 29 patients (39 lesions) previously treated with stereotactic radiation surgery or whole-brain radiation therapy for brain metastasis who currently had at least 1 contrast-enhancing lesion on MR imaging. All patients underwent ^{18}F-FET PET imaging, and the results were classified by kinetic uptake patterns as: pattern 1, constantly increasing time–activity curve (TAC); pattern 2, stable TAC, early peak (<20 minutes after injection) followed by plateau; and pattern 3, decreasing TAC, early peak (<20 minutes after injection) followed by decrease. For analysis, patterns 2 and 3 were grouped together and compared with pattern 1. Histology and follow-up determined that 32 lesions (82%) were recurrent metastases and 7 (18%) represented radiation necrosis. The researchers showed that accuracy for correct identification of recurrent brain metastases was only 54% using static tumor-to-background ratios (TBRs). This percentage rose to 72% for TAC patterns 2 and 3 compared with TAC pattern 1. The authors achieved 100% specificity when TBR was >2.37 in lesions categorized as patterns 2 or 3. However, combining TBR and uptake patterns did not improve diagnostic accuracy. Although these are promising data, it is clear that there is room for more work with other tracers and/or approaches in the setting of differentiating brain metastases from necrosis.

Another interesting target in cancer is the α-chemokine receptor CXCR4. Wang et al. from the Fourth Military Medical Hospital (Xi'an, China) and the National Institute of Biomedical Imaging and Bioengineering (Bethesda, MD) reported on a "Prospective study of ^{68}Ga-NOTA-NFB: radiation dosimetry in healthy volunteers and first application

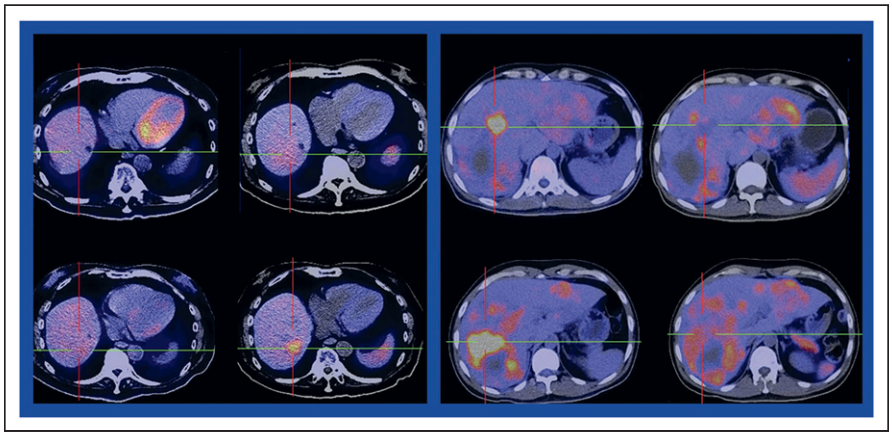

FIGURE 1. Baseline ^{18}F-FDG and ^{11}C-acetate PET/CT and prediction of treatment response/survival in intermediate grade hepatocellular carcinoma (HCC) patients treated with ^{90}Y-selective internal radiotherapy. Left block: Follow-up (top) and baseline (bottom) ^{18}F-FDG (left) and ^{11}C-acetate (right) PET/CT images from a patient with ^{11}C-acetate–avid HCC who went on to a good treatment response, with survival >24 mo. Right block: Corresponding images from a patient with ^{18}F-FDG–avid HCC but without baseline ^{11}C-acetate avidity who had a poor response and who died 9 mo after treatment.

in glioma patients" [11]. CXCR4 is overexpressed in various types of human cancer. As a specific imaging agent for CXCR4, ^{68}Ga-NOTA-NFB was investigated to assess its safety, biodistribution, and dosimetric properties in 6 healthy volunteers and to preliminarily evaluate its application in 8 patients with glioma. Figure 2 shows a comparison of MR (top), ^{18}F-FDG PET (middle), and ^{68}Ga-NOTA-NFB PET (bottom) imaging in 3 patients with (left to right) grades 2, 3, and 4 glioma. In grade 2 glioma, where there is not a blood–brain barrier breakdown, no uptake is seen, which may be a reflection of delivery. Images from grades 3 and 4 clearly show that CXCR4 expression is targeted by ^{68}Ga-NOTA-NFB. This tracer has the potential not only for use in initial detection and tumor assessment but for in situ tumor characterization of changes and to help guide therapy and responsiveness. Many of our new tracers have these multilevel goals: to provide not only better diagnosis, staging, and monitoring but also useful characterization of tumors in situ.

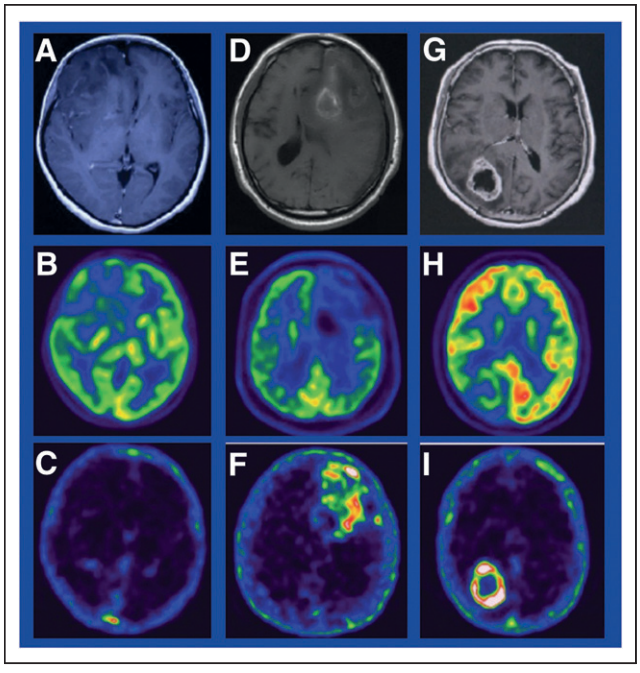

FIGURE 2. Comparison of MR (A, D, G), ^{18}F-FDG PET (B, E, H), and ^{68}Ga-NOTA-NFB PET (C, F, I) imaging in 3 patients with grades 2 (A, B, C), 3 (D, E, F), and 4 (G, H, I) glioma.

Lapa et al. from Würzburg University (Germany) and the Technische Universität München (Germany) reported on "First in man experience of CXCR4-directed endoradiotherapy with ^{177}Lu- and ^{99}Y-labeled pentixather in multiple myeloma patients" [14]. The group used their CXCR4 ligand not only for imaging but also for radiotherapy. The group has previously reported on ^{68}Ga-pentixafor (pentixather) in a number of human malignancies, including lymphoma, chronic lymphocytic leukemia, and multiple myeloma. In multiple myeloma, ^{68}Ga-pentixafor for PET has shown encouraging results in comparison to ^{18}F-FDG PET, including identification of patients for CXCR4-directed treatment and peptide receptor radiotherapy (PRRT). Development of derivatives of the group's original compound allowed labeling with a range of α and β emitters. Their theranostic approach used 2 β emitters: ^{177}Lu and ^{99}Y. Figure 3 shows encouraging responses in 2 patients. Before ^{177}Lu-pentixather treatment, patient 1 (left) showed sites of CXCR4 expression and uptake on ^{68}Ga-pentixafor, correlating well with uptake on ^{18}F-FDG (next right), which indicated numerous osseous sites involved. Two weeks after ^{177}Lu-pentixather administration ^{18}F-FDG PET showed a good partial response. In the second patient (right), pretreatment imaging showed overexpression of CXCR4 before therapy, correlating reasonably well with ^{18}F-FDG uptake, with a complete response after ^{177}Lu-pentixather treatment. The authors concluded that, in combination with high-dose chemotherapy and autologous stem cell transplantation, CXCR4-targeted PRRT with pentixather is a promising new option for patients with advanced multiple myeloma. We are rapidly expanding our armamentarium of theranostic agents. We began with iodine, the historical mainstay of nuclear medicine, and we have had excellent work with somatostatin receptors as well as prostate-specific membrane antigens (PSMAs). This paper and others at the Annual Meeting made it clear that

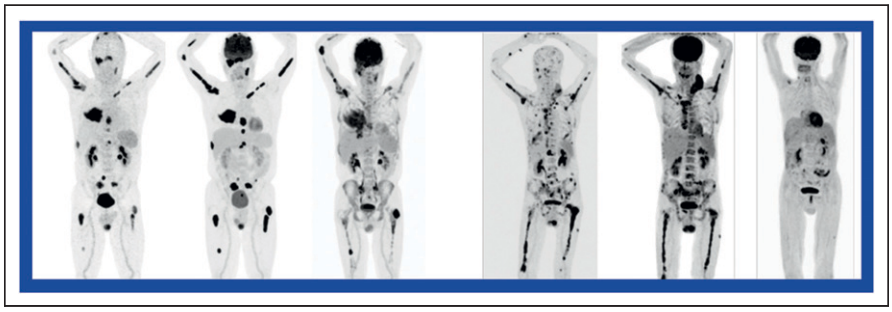

FIGURE 3. CXCR4-directed endoradiotherapy with ^{177}Lu- and ^{99}Y-labeled pentixather in 2 patients with multiple myeloma. Left 3 images: Before ^{177}Lu-pentixather treatment, patient showed sites of CXCR4 expression and uptake on ^{68}Ga-pentixafor (left), correlating well with uptake on ^{18}F-FDG (next right), which indicated numerous osseous sites involved. Two weeks after ^{177}Lu-pentixather administration ^{18}F-FDG PET (right) showed a good partial response. Right 3 images: In a second patient, pretreatment ^{68}Ga-pentixafor imaging showed overexpression of CXCR4 before therapy (left), correlating with ^{18}F-FDG uptake (middle), with a complete response 2 wk after ^{177}Lu-pentixather treatment (right).

vigorous investigations are underway in other cancers and other agents to explore the potential of combined theranostics.

Another study from Chen et al. from Hong Kong Sanatorium and Hospital and the University of Hong Kong, this one looking at myeloma and at the prognostic value of imaging, reported that "^{11}C-acetate PET/CT predicts 4-year overall survival for patients with newly diagnosed myeloma" [657]. In a population of 20 patients with multiple myeloma (13 stage I, 3 stage II, 4 stage III by the International Staging System), ^{11}C-acetate PET/CT was positive in 18 (90%) and ^{18}F-FDG was positive in 12 (60%). During 4 years of follow-up, 8 (40%) patients died. Subsequent analysis identified 2 significant predictors of overall survival: pretreatment generalized marrow activity (maximum standardized uptake value [SUV_{max}] on L3) assessed by ^{11}C-acetate PET/CT and pretreatment serum β-2 microglobulin levels. Patients with diffuse uptake at baseline had much poorer outcomes than patients who had less uptake in the marrow. Figure 4 shows example images from 2 patients, with ^{11}C-acetate PET images on the left in each set and ^{18}F-FDG PET images on the right. For the patient on the left, L3-measured generalized marrow activity was 5.6 for ^{11}C-acetate and 2.7 for ^{18}F-FDG PET. This patient survived for 27 months. L3-measured generalized marrow activity was 3.6 for ^{11}C-acetate and 2.7 for ^{18}F-FDG PET in the patient on the right, for whom survival was >4 years. ^{18}F-FDG uptake was the same in these patients, but ^{11}C-acetate appeared to correlate with outcome in these representative examples.

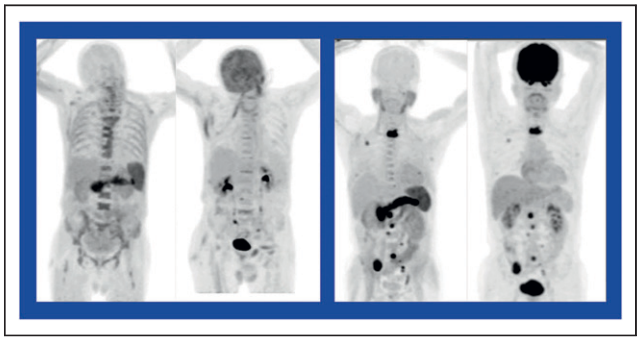

FIGURE 4. ^{11}C-acetate PET/CT in newly diagnosed myeloma. Left block: Patient in whom L3-measured generalized marrow activity (GMA) was 5.6 for ^{11}C-acetate (left) and 2.7 for ^{18}F-FDG PET (right) and who survived for 27 mo. Right block: Patient in whom L3-measured GMA was 3.6 for ^{11}C-acetate (left) and 2.7 for ^{18}F-FDG PET (right) and who survived for more than 4 y.

Much recent work has focused on theranostic applications based on PSMA as a target. Kulkarni et al. from the Zentralklinik Bad Berka (Germany) and Technische Universität München (Germany) reported on "Therapy of metastasized castrate-resistant prostate cancer using ^{177}Lu-labeled DOTAGA-PSMA small molecules: first clinical results in a larger patient cohort" [10]. Figure 5 shows patients with diffuse metastases who have responded well to ^{177}Lu therapy. ^{177}Lu can be directly imaged with SPECT/CT to monitor tumor dose delivery. In this safety and efficacy study, the researchers reported on ^{177}Lu-PSMA therapy results in 60 patients with a total of 142 cycles (2–5 per patient), a mean administered radioactivity of 8.7 GBq per cycle, and a mean follow-up of 12 months (range, 3–25 months). Response was measured according to molecular response criteria on ^{68}Ga-PSMA PET/CT, correlating with a fall in prostate-specific antigen (PSA) after therapy (Fig. 6). No hematologic, renal, or salivary toxicities were noted, and improvements in quality of life and pain scores were noted in all patients. After 2–4 cycles of therapy, the researchers noted 1 patient with molecular complete remission, 13 with partial remissions, 2 with stable disease, and 9 with progressive disease. Progression-free survival was 14 months, and the overall survival median was not reached over the 15 months of the study, which are exciting results in patients with these very advanced cancers. The authors concluded that peptide radioligand therapy using ^{177}Lu-labeled DOTAGA-based PSMA small molecules is safe and effective in castrate-resistant metastatic prostate cancer and potentially may confer survival benefits when compared with conventional therapy regimens.

A number of different and new-generation PSMA-targeting agents are under investigation. Benesova et al. from the German Cancer Research Center (Heidelberg) and University Hospital Heidelberg (Germany) reported on "PSMA-617—a novel theranostic PSMA inhibitor for both diagnosis and endoradiotherapy of prostate cancer" [63]. This group has identified a theranostic PSMA inhibitor which they have labeled

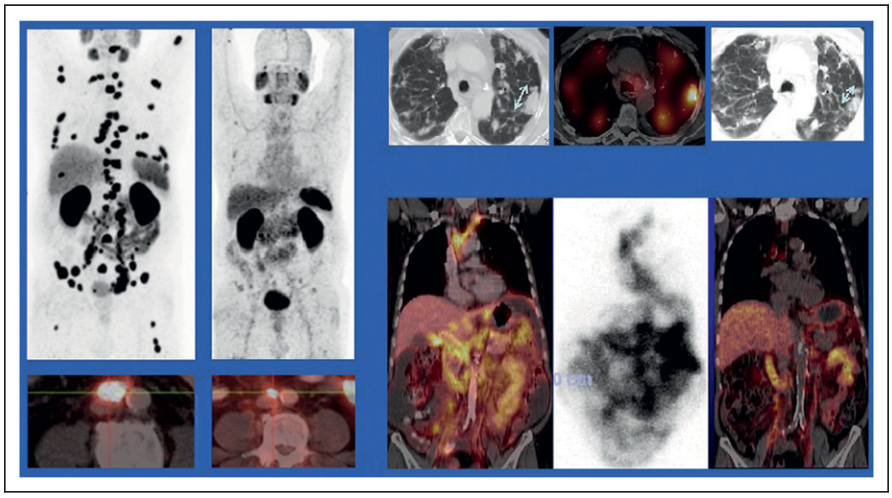

FIGURE 5. ^{177}Lu-labeled DOTAGA-PSMA small molecule therapy in metastasized castrate-resistant prostate cancer. Left block: Example pre- (left) and post- (right) therapy PET (top) and PET/CT images (bottom). Significant decrease (89%) noted in SUV_{max} of target lesion (paraaortic lymph node) and in size on CT. Right block top: CT response in lung metastasis: left, CT before therapy; middle, ^{177}Lu-PSMA SPECT/CT at 118 h; right, CT after therapy. Right block bottom: biochemical and imaging response in prostate cancer with pleuroperitoneal metastases, before (left) and after (right) therapy.

with both diagnostic and therapeutic radiometals. They described their agent, PSMA-617, and its development with respect to preclinical tumor targeting and pharmacokinetics, along with clinical diagnostic scanning with ^{68}Ga-PSMA-617 PET/CT and results from a patient treated with ^{177}Lu-PSMA-617. Figure 7 shows these preliminary imaging and treatment results. The ^{68}Ga-PSMA-617 PET/CT images (left) show very high uptake in the lymph nodes, providing excellent TBRs and helping to identify small lesions. This imaging approach will also be useful in identifying those patients likely to benefit from treatment with the ^{177}Lu-labeled agent. On the right, baseline and restaging images after ^{177}Lu-PSMA-617 treatment show a remarkable response and decrease in uptake, correlating with a change in PSA levels. Pioneering work in coupling peptide-targeted radiotherapy with imaging for somatostatin receptors in carcinoids and neuroendocrine tumors has now been transferred with extraordinary promise in prostate cancer among several different groups, and we are likely to see additional significant advances in this area in the near future.

Many approaches are possible in improving prostate cancer imaging. Pandit-Tasker et al. from Memorial Sloan–Kettering Cancer Center (New York, NY) and ImaginAb Inc. (Inglewood, CA) reported on "First-in-human ^{89}Zr-Df-IAB2M anti-PSMA minibody in patients with metastatic prostate cancer" [400]. The study included 28 patients who underwent standard imaging (CT/MR and bone scan), ^{18}F-FDG PET imaging, and PET imaging with various doses of ^{89}Zr-Df-IAB2M. A total of 19 biopsies (10 soft tissue, 9 bone) were performed in 18 patients. Figure 8 shows that the novel agent identified with high TBRs more metastatic sites than ^{18}F-FDG PET or bone scanning. In lesional detection comparisons, ^{89}Zr-IAB2M PET, ^{18}F-FDG PET, CT, and bone scan detected 228 (81.7%), 73 (26.2%), 148 (53.1%), and 161 (57.7%), respectively, of identified bone lesions. The figures for soft tissue lesion detection were 98 (85.9%) for ^{89}Zr-IAB2M PET, 55 (48.2%) for ^{18}F-FDG PET, and 75

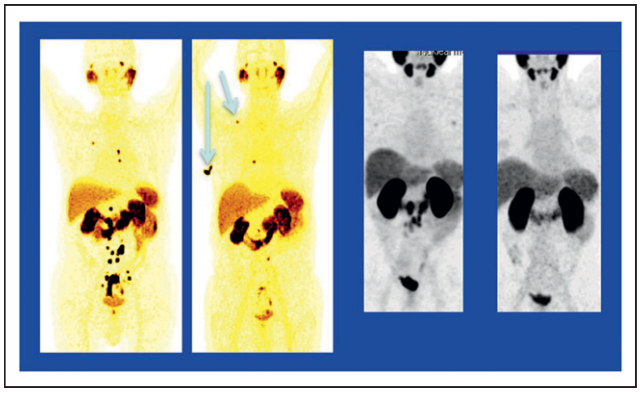

FIGURE 6. ^{177}Lu-labeled DOTAGA-PSMA small molecule therapy in metastasized castrate-resistant prostate cancer. Left block: Pre- (left) and post- (right) therapy imaging. Right block: Pre- (left) and post- (right) therapy PET imaging shows molecular complete remission.

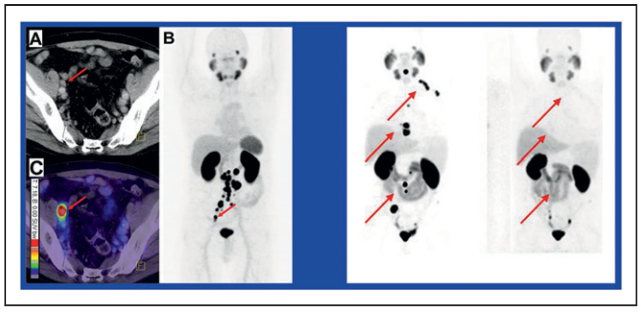

FIGURE 7. PSMA-617 for diagnosis and endoradiotherapy in prostate cancer. Left block: ^{68}Ga-PSMA-617 PET/CT. A: CT demonstrating multiple lymph node metastases; B: coronal maximal-intensity projection; C: fusion of PET and CT. Red arrows point to representative lesion. Right block: Pre-(left) and post-(right) ^{177}Lu -PSMA-617 treatment images acquired with ^{68}Ga-PSMA-11 PET show a marked radiologic response (red arrows). PSA level in blood decreased from 38.0 to 4.6 ng/mL.

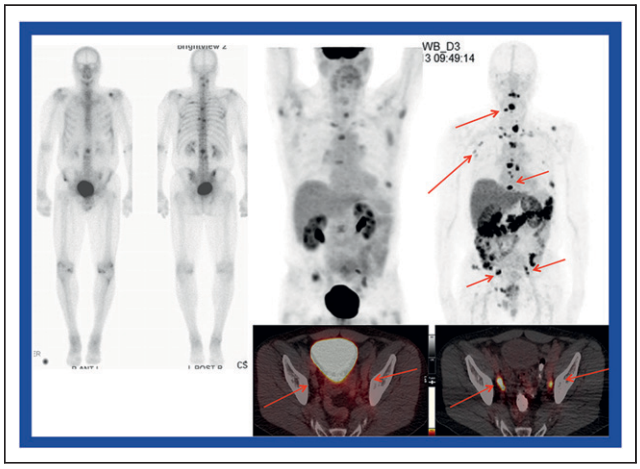

FIGURE 8. ^{89}Zr-Df-IAB2M anti-PSMA minibody in metastatic prostate cancer. Left: Bone scan images in a patient with prostate-specific antigen of 40.5 and Gleason score of 9. Right: ^{18}F-FDG PET (top left) and PET/CT (bottom left) and ^{89}Zr-Df-IAB2M PET (top right) and PET/CT (bottom right) imaging in the same patient. Multiple lesions (arrows) not visualized on ^{18}F-FDG PET were evident on ^{89}Zr-Df-IAB2M PET.

(65.8%) for CT. A total of 65 unique bone and 32 soft tissue sites were identified only by ^{89}Zr-IAB2M PET. ^{89}Zr-IAB2M PET had a high concordance (89.5%) with true-positives and true-negatives at biopsy. This again points to the fact that there are many promising approaches for assessment of prostate cancer and that there is no single "right" way to image. Multiple approaches bring new insights into both the most promising treatment strategies and to our basic understanding of various pathway targets in the disease.

Mena et al. from Johns Hopkins University/Applied Physics Laboratory (Baltimore, MD) and the University of Wisconsin (Madison) reported on "First-in-man analysis of ^{18}F-DCFPyL, a second generation, ^{18}F-labeled PSMA-targeted radiotracer, in patients with metastatic prostate cancer" [399]. The authors reported on initial clinical experience with this agent and compared tumor uptake with that of ^{18}F-DCFBC, the first radiofluorinated PSMA-targeted small molecule for PET imaging of prostate cancer. Figure 9 shows high uptake over time using this new agent. The researchers documented rapid, high accumulation in primary tumor, lymph nodes, and sites of bone metastasis. Physiologic accumulation corresponded to distribution of PSMA, with relatively prompt excretion of radiotracer. The median SUV_{max} of ^{18}F-DCFPyL was 2.0 times higher than that for ^{18}F-DCFBC for nodal disease and 13.6 times that for bony lesions. Tumor-to-liver, tumor-to-blood, and tumor-to-muscle ratios were also significantly higher with ^{18}F-DCFPyL than with the first-generation compound. This method of targeting PSMA has the advantages of a fluorine probe and a small molecule.

Malignancies in Women

Grootendorst et al. from King's College London (UK) reported on the "Clinical feasibility of intraoperative ^{18}F-FDG Cerenkov luminescence imaging (CLI) in breast cancer surgery" [13]. As part of a clinical trial focusing on breast-conserving surgery, the authors looked at the feasibility of intraoperative CLI evaluation of tumor excision margins and sentinel lymph node (SLN) metastases. Patients were injected with 5 MBq/kg ^{18}F-FDG 1–2 hours before surgical excision of tumor and SLNs. Tumors and SLNs were split and imaged intraoperatively with CLI immediately after excision, a procedure that required <5 minutes. Figure 10 shows an example with tumor resection margins clearly identified. No evidence of radioactive contamination was found outside the operative field. The authors also looked at radiation dose to patients, surgeons, and staff with the procedure. In the United Kingdom, surgeons could potentially perform 93 such procedures per year before exceeding the annual whole-body radiation dose constraint of 6,000 μSv. In the United States, 1,000 procedures could potentially be performed because of the higher allowable radiation dose of 50,000 μSv. The authors concluded that intraoperative ^{18}F-FDG CLI is a feasible and low-risk procedure.

Wang et al. from the Massachusetts General Hospital (Boston), the Memorial Sloan–Kettering Cancer Center (New York, NY), Vanderbilt University (Nashville, TN), and Seragon Pharmaceuticals (San Diego, CA) reported

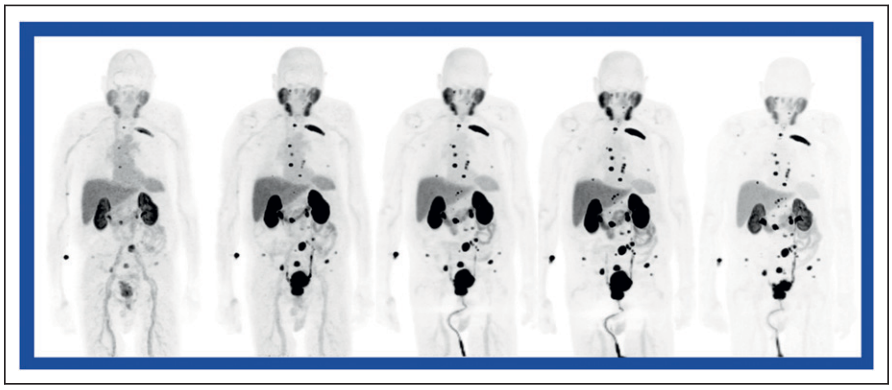

FIGURE 9. PSMA-targeted PET of metastatic, castration-resistant prostate cancer with ^{18}F-DCFPyL. PET imaging at (left to right) 0, 10, and 30 min and 1 and 2 h demonstrated rapid and very high accumulation of ^{18}F-DCFPyL at primary tumor site and lymph node as well as in bony metastatic disease, with high tumor-to-background ratio. Physiologic distribution of the radiotracer was seen in salivary glands, liver, small bowel, and kidneys/bladder.

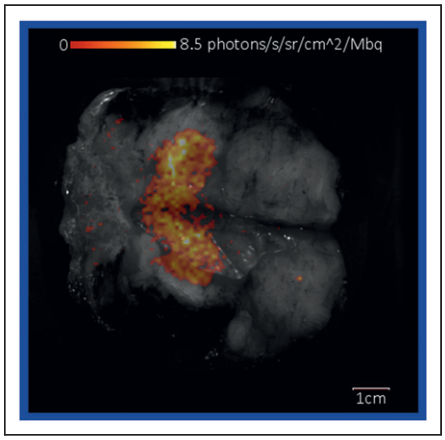

FIGURE 10. Intraoperative Cerenkov luminescence imaging of incised wide local excision specimen in breast cancer surgery. Elevated radiance (8.26, ROI SD 1.2) was seen in this 32-mm, HER2-negative/estrogen receptor–negative grade 3 invasive ductal carcinoma. Tumor-to-healthy tissue background ratio was 3.18. Tumor resection margins were clear (≥3mm). Imaging procedure time was 5 min.

on "Validation of target engagement using ^{18}F-fluoroestradiol (^{18}F-FES) PET in patients undergoing therapy with selective estrogen receptor (ER) degrader, ARN-810 (GDC-0810)" [565]. The researchers were seeking to identify when a sufficient dose of the therapeutic agent had been delivered to degrade the ER, by applying ^{18}F-FES PET to validate ER target engagement. Thirty patients underwent baseline and intertreatment imaging. The number of ^{18}F-FES–avid lesions on baseline ranged from 1 to >10, with SUV_{max} ranging from 1.5 to 17.2. All except 3 posttherapy ^{18}F-FES scans showed complete or near complete (>90%) suppression of ^{18}F-FES uptake to background levels, indicating that ARN-810 is effective in degrading the ER sites. Figure 11 (top) shows a patient with widespread ^{18}F-FES–avid and ERα mutant skeletal metastases at baseline and during treatment with ARN-810. Figure 11 (bottom) shows a patient with ^{18}F-FES–avid soft tissue metastases. This successful imaging of target engagement has promise not only for identifying patients who are more likely to respond to specific therapies but for guiding therapeutic drug dosing in individual patients.

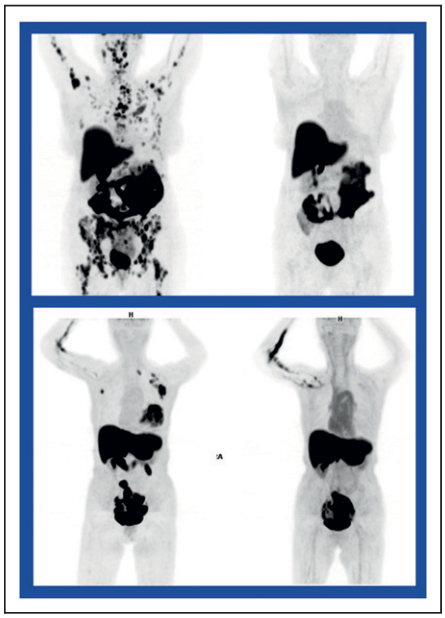

FIGURE 11. ^{18}F-FES PET imaging to validate estrogen receptor target engagement in patients undergoing therapy with ARN-810. Top: Patient with widespread ^{18}F-FES–avid and ERα mutant skeletal metastases at baseline and during treatment with ARN-810. Bottom: Patient with ^{18}F-FES–avid soft tissue metastases and at treatment trough with ARN-810.

Tsujikawa et al. from the University of Fukui (Japan) reported on "Assessment of hormone sensitivity in uterine leiomyoma patients using ^{18}F-FES PET" [345]. In the study, 10 patients with uterine leiomyomas underwent ^{18}F-FES PET, ^{18}F-FDG PET, and pelvic MR imaging before treatment, as well as follow-up MR imaging after 1–6 cycles of gonadotropin-releasing hormone treatment. Pretreatment tracer uptake was compared with volume reduction after therapy. Figure 12 shows the variety of ER expression in leiomyoma, with corresponding different levels of uptake. Volume after treatment corresponded quite nicely with ^{18}F-FES uptake. The authors concluded that pretreatment ^{18}F-FES SUV and ^{18}F-FES/^{18}F-FDG ratio can be used for predicting gonadotropin-releasing hormone sensitivity in uterine leiomyoma patients before treatment and that more accurate prediction may be provided in evaluation of intramural leiomyomas.

Tade et al. from Emory University (Atlanta, GA) and Loyola University (Chicago, IL) reported on "Preliminary findings of anti-^{18}F-FACBC PET-CT imaging of breast cancer" [567]. Previous reporting on anti-1-amino-3-^{18}F-fluorocyclobutane-1-carboxylic acid (^{18}F-FACBC) PET has focused mainly on prostate cancer. In this study, the goal was to characterize amino acid transport via ^{18}F-FACBC PET/CT in benign and malignant breast lesions and correlate these results with histologic characteristics. The study included 12 women (mean age, 64 y; range, 49–89 years). The researchers noted significantly higher ^{18}F-FACBC uptake in malignant breast tumors than in benign tumors at all imaging time points. The highest uptake was found in invasive metaplastic carcinoma when compared to other pathologic subtypes of breast cancer. Figure 13 shows examples with a high degree of ^{18}F-FACBC uptake in a patient with disease recurrence and in a patient with newly diagnosed breast cancer. Figure 14 compares ^{18}F-FACBC uptake in benign and malignant lesions. The authors concluded that ^{18}F-FACBC shows promise in delineating malignant from benign breast lesions and correlates with histologic subtypes of breast cancer.

Interest in radioimmunotherapy continues to grow. Meredith et al. from the University of Alabama School of Medicine (Birmingham), ArevaMed (Bethesda, MD), and Dade Moeller Health Group (Richland, WA) reported on "Safety of first-in-human intraperitoneal α radioimmunotherapy with ^{212}Pb-TCMC-trastuzumab" [283]. The purpose of the study was to determine the long-term safety of salvage intraperitoneal ^{212}Pb-TCMC-trastuzumab therapy in patients with HER2-expressing malignancy. Follow-up included toxicity and other monitoring for 1 year. The

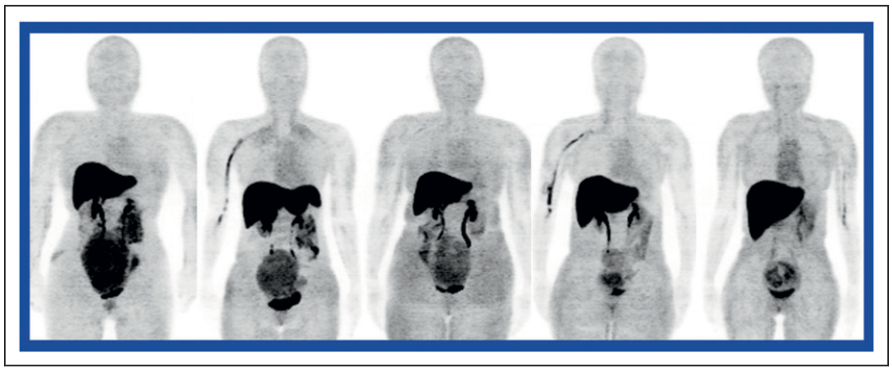

FIGURE 12. ^{18}F-FES PET and range of estrogen receptor expression images (coronal maximal-intensity projection) in 5 patients with uterine leiomyoma.

researchers found minimal distribution of radioactivity outside the abdominal cavity, with no excess organ uptake. With escalation over 6 dose levels, minimal early agent-related toxicity was noted, with no late toxicity in the 16 patients studied. Safety data were deemed adequate for further study of this agent. The researchers noted a trend toward lower tumor markers and greater tumor regression with higher doses. Figure 15 shows anterior and posterior abdominal retention images immediately and 18 hours after injection of the ^{212}Pb-TCMC-trastuzumab. A number of radioimmunotherapy trials are currently underway, looking at both α and β emitters.

Sörenson et al. from Uppsala University (Sweden), Affibody AB (Stockholm, Sweden), and Akademiska Hospital (Uppsala, Sweden) reported on "Accuracy of ^{68}Ga-ABY-025 PET/CT for determination of HER2-expression in metastatic breast cancer" [156]. Their goal was to optimize peptide mass and scan timing in 10 patients with repeated scanning with this ^{68}Ga-labeled affibody. The researchers found that a higher mass of unlabeled peptide (~430 vs ~80 μg) decreased uptake in liver and increased SUV in HER2-positive metastases. All HER2-positive lesions were visualized at 2 hours after injection with the high peptide dose. SUV_{max} in metastases and tumors at biopsy at 2 hours were 11.6 ± 5.2

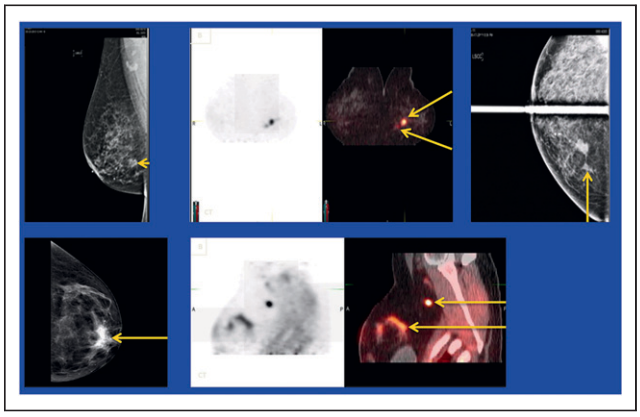

FIGURE 13. ^{18}F-FACBC PET/CT in breast cancer. Top: 67-y-old woman with disease recurrence in left breast. Left: Single breast lesion identified on mammogram; biopsy-proven as invasive ductal carcinoma grade 2. Middle images: ^{18}F-FACBC PET and PET/CT demonstrated uptake in the primary lesion and an additional subcentimeter satellite lesion Right: Subsequent repeat mammogram showed same subcentimeter satellite lesion. Bottom: 49-y-old with newly diagnosed breast cancer. Left: Biopsy-proven invasive lobular carcinoma seen on mammogram with no nodal involvement. Middle: ^{18}F-FACBC PET. Right: Sagittal view of ^{18}F-FACBC PET/CT demonstrates intense uptake in the primary lesion with metastasis to a axillary lymph node.

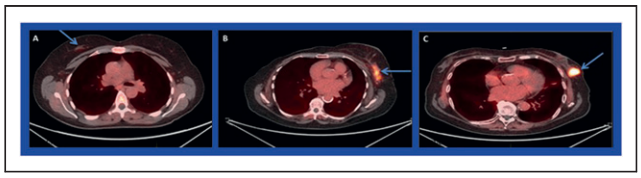

FIGURE 14. ^{18}F-FACBC uptake on PET/CT in benign and malignant lesions. Left: Ductal hyperplasia; SUV_{max} at 5 min = 2.0. Middle: Invasive lobular carcinoma; SUV_{max} at 5 min = 6.6. Right: Invasive ductal carcinoma; SUV_{max} at 5 min = 8.8.

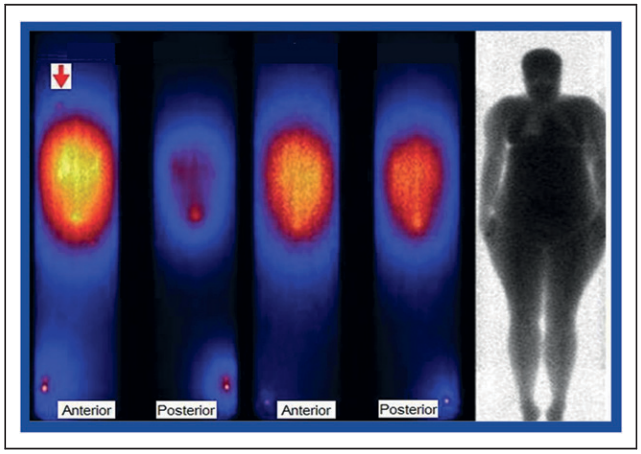

FIGURE 15. ^{212}Pb-TCMC-trastuzumab abdominal retention images acquired immediately (left 2 images) and at 18 h (right 2 images) after injection in a patient with HER2-expressing malignancy.

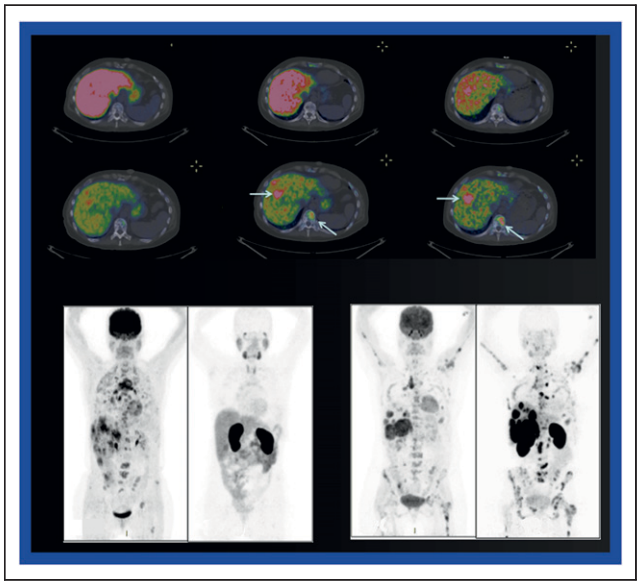

FIGURE 16. ^{68}Ga-ABY-025 PET/CT and effect of peptide mass and scan timing for determination of HER2-expression in metastatic breast cancer. Top block: Low-dose (top row; 78 ± 8 μg injected peptide) and high-dose (bottom row; 427 ± 19 μg injected peptide) images (left to right) at 1, 2, and 4 h (1 wk interval between low- and high-dose scanning). Arrows show gradually improved appearance of lesions in liver and bone at higher peptide doses and longer times post injection. Bottom block: All patients were scanned with ^{18}F-FDG PET (left images) prior to ^{68}Ga-ABY-025 imaging to document location of viable metastases. Left: Maximum-intensity projection images thresholded to an SUV of 10 in a patient with disseminated disease in soft tissues and bone. Metastatic ^{68}Ga-ABY-025 uptake (right) was minimal (SUV_{max} range 0–4), confirming HER2-negative status. Physiologic uptake was seen in salivary and lacrimal glands, thyroid, and intestines. Right: Patient with HER2-positive primary tumor with disseminated disease to liver and bone. ^{68}Ga-ABY-025 PET (right) shows intense metastatic uptake (SUV_{max} range 4–64), resulting in a "superscan" with minimal physiologic uptake. Patient progressed on all therapy, including anti-HER2 targeting.

in HER2-positive patients and 2.6 ± 2.2 in HER2-negative patients. At 4 hours these figures were 15.0 ± 3.4 and 2.7 ± 2.1, respectively. Test–retest reproducibility using the high peptide dose and scanning at 2 hours in 5 patients with a 1-week interval showed an intraclass correlation of SUV_{max} and a high repeatability coefficient. These results served to guide treatment. Anti-HER2 treatment was canceled in 1 patient and initiated in 2 patients as a result of receptor up- or downregulation. Figure 16 shows an example of ^{68}Ga-ABY-025 PET/CT imaging in metastatic breast cancer. The effect of peptide mass and scan timing can be seen in images of liver uptake from low- and high-dose peptide. Less liver uptake is seen with the higher peptide dose, which helped to identify hepatic metastases that would not otherwise have been visualized. The comparison with ^{18}F-FDG imaging is quite marked, another example of the maxim that when 2 tracers provide different results in the same patient, the mechanism of action of tracer accumulation is likely to be different. Immunohistochemistry also showed good correlation with ^{68}Ga-ABY-025 PET/CT imaging, and no safety issues were noted. The authors concluded that ^{68}Ga-ABY-025 PET/CT accurately assessed HER2 receptor status in metastatic breast cancer.

Conclusion

This year's SNMMI Annual Meeting presentations continued to demonstrate the vibrant nature of our field in approaching the era of precision medicine and pathway-specific targeted therapy in oncology. Continued growth in imaging targets, theranostics, and first-in-human use of radiotracers and radiotherapeutics highlights the integral contributions we have made and will continue to make in the oncologic treatment paradigms of today and tomorrow.